Supplement of Solid Earth, 11, 2221–2244, 2020
https://doi.org/10.5194/se-11-2221-2020-supplement
© Author(s) 2020. This work is distributed under
the Creative Commons Attribution 4.0 License.

Solid Earth Open Access EGU

Supplement of

Fracture attribute scaling and connectivity in the Devonian Orcadian Basin with implications for geologically equivalent sub-surface fractured reservoirs

Anna M. Dichiarante et al.

Correspondence to: Ken J. W. McCaffrey (k.j.w.mccaffrey@durham.ac.uk)

The copyright of individual parts of the supplement might differ from the CC BY 4.0 License.

Testing Fracture Distributions

Mitzenmacher (2004) showed that difference in the tail of the power-law, log-normal and double Pareto (a distribution with the body of a log-normal and tail of power-law distribution) are may be better visualized in complementary cumulative distribution plots at logarithmic scale (ccdf, **Fig. S1**). Legitimate data points (data occurring in the yellow box in **Fig. S1**) are well fitted by power-law, log-normal and double Pareto distribution (Mitzenmacher, 2004). However, when data are affected by censoring and truncation effects, the power-law distribution type shows the least similarity to the biased data. More specifically, when datasets include truncated data (blue box in **Fig. S1**), both log-normal and double Pareto distributions fit the data (see Truncation blue box in **Fig. S1**a) and therefore it is not correct to base the distribution choice on these biased data (Mitzenmacher, 2004).

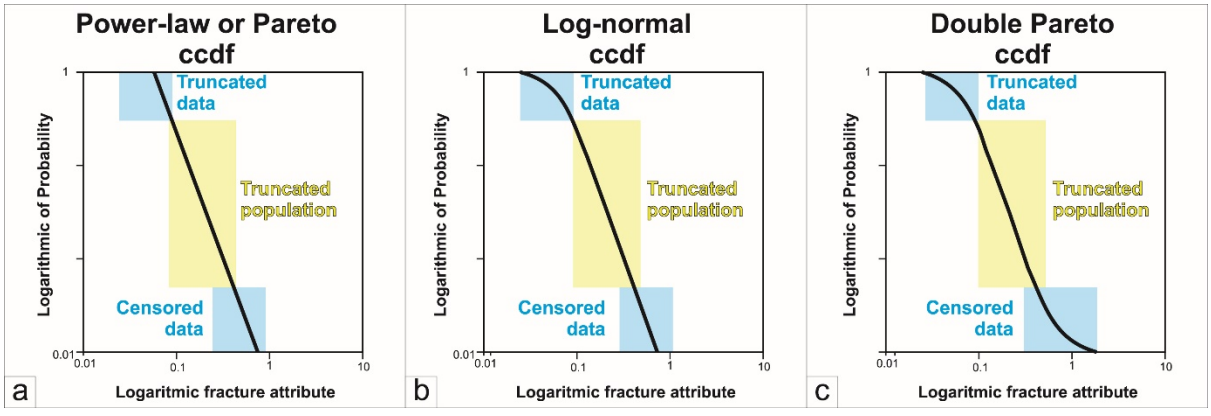

Fig S1: Sketch showing the similarity in the shape of (a) power-law, (b) log-normal and (c) double pareto complementary cumulative distribution function (ccdf) as illustrated in Mitzenmacher (2004). The yellow region represents the truncated part of the population that do not suffer of truncation and censoring biases, blue regions represent truncated and censored data.

1.1.1 Maximum likelihood estimator (MLE) and Kolmogorov-Smirnoff (KS)

The determination of which type of population is most likely to have generated the sample recorded is a key part of any fracture attribute analysis (Rizzo et al., 2017). As pointed out by Clauset et al. (2009), use of the maximum likelihood estimator (MLE) should be preferred over use of least square regression analyses (R^2) for the fitting of power-law distributions because a power-law may appear to be a good fit even when the data are non-power-law. Rizzo et al. (2017) performed the MLE on power-law, log-normal and exponential distributions by using a suite of custom MATLAB™ functions, integrated into FracPaQ (Healy et al., 2017). They compared the MLE to the linear regression method for synthetic data in order to demonstrate the validity and ability of this approach to correctly estimate statistical parameters. The MLE approach maximizes the likelihood, gives estimate of the governing parameters (α for power-law distribution, λ for exponential distribution and μ and σ for the log-normal distribution) of the different fitting equations:

Power-law: $$p(x|\alpha) = \frac{\alpha-1}{x_{\min}}\left(\frac{x}{x_{\min}}\right)^{-\alpha} \quad \text{Eq. 1}$$

Log-normal: $$p(x|\mu,\sigma) = \frac{1}{x\sigma\sqrt{2\pi}}\exp\left(-\frac{(\ln x-\mu)^2}{2\sigma^2}\right) \quad \text{Eq. 2}$$

Exponential: $$p(x|\lambda) = \lambda\exp(-\lambda x) \quad \text{Eq. 3}$$

where $x_{\min}$ in the power-law distribution, is a required parameter representing the lower bound below which the power-law distribution is not valid (Clauset et al., 2009). The $x_{\min}$ parameter can be estimated using the Kolmogorov-Smirnoff (KS) test which minimizes the difference between the data and the synthetic data generated using the parameter derived from the MLE (Clauset et al., 2009; Rizzo et al., 2017). Two percentage outputs are obtained from the MLE method. The P-percentage (PP) and H-percentage (HP) are the percentages of the *p*-value larger than 0.05 over the total *n*-cycles and the percentage of the H0 (null

hypothesis) result over the total *n*-cycles, respectively. If the *p*-value is less than or equal to 0.05, the test suggests that "the observed data are inconsistent with the null hypothesis, so the null hypothesis must be rejected, while if the *p*-value is far from zero and close to 1, the observed data are not inconsistent with the null hypothesis, and the chosen fitting method can be applied" (Hung et al., 1997). However having a *p*-value larger than 0.05, does not prove that the tested hypothesis is true. Clauset et al. (2009) have shown that the *p*-value for alternative distributions can be calculated to test against other possibilities.

When testing the entire sample we might obtain misleading fitting results because we have included censored and truncated data. On the other hand, when testing truncated populations we could be removing legitimate points and increasing the error; for example, if the upper cut is too high (x_{min} too high) (Clauset et al., 2009). In order to address this problem, the methodology proposed by Rizzo et al. (2017) and used by FracPaQ (Healy et al., 2017), was implemented here by calculating the MLE on progressively truncated populations for power-law, exponential and log-normal distributions. Knowing that attributes collected from outcrop are naturally affected by truncation and censoring bias, we performed the MLE and KS test and calculated the PP and HP for truncated populations defined by progressive variation in the upper cut (uc) and lower cut (lc). 40 values of censoring for both uc and lc were considered, resulting in 800 simulations. The resulting values of percentages (HP and PP) were visualized in two lc vs. uc checkerboard-like plots (e.g. **Fig. S2**). The best-fit results in the highest percentage values obtained, with the minimum lower and upper cuts (red colours in **Fig. S2** and corresponding distribution plot in **Fig. S3**). This methodology is more robust than the very commonly used visual estimation (**Fig. S2**). Such an analysis shows that the upper cut (lower values) has a consistently greater influence over the population fit compared to the lower cut (see **Fig. S2** and percentages reported in Tables 3 and 4).

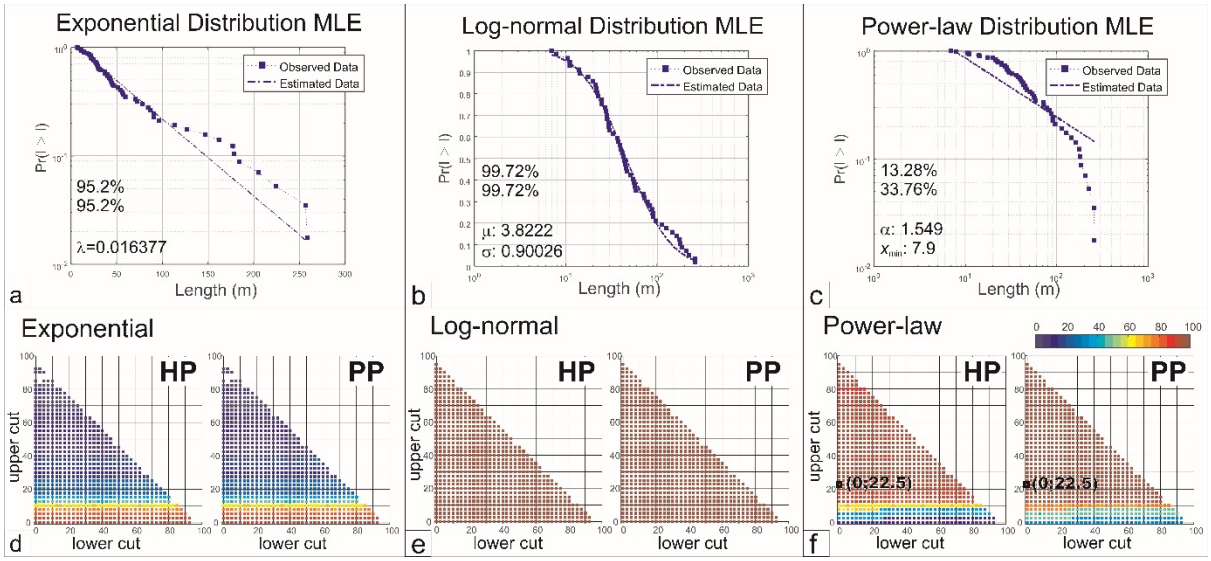

Fig. S2: (Top) Example of MLE for (a) exponential, (b) log-normal and (c) power-law distributions for the entire length population; (Bottom) "Checkerboard" diagrams showing the values of HP and PP for (d) exponential, (e) log-normal and (f) power-law distributions of progressively truncated population. Data are from the transect at St. John's Point (SJ) in this study.

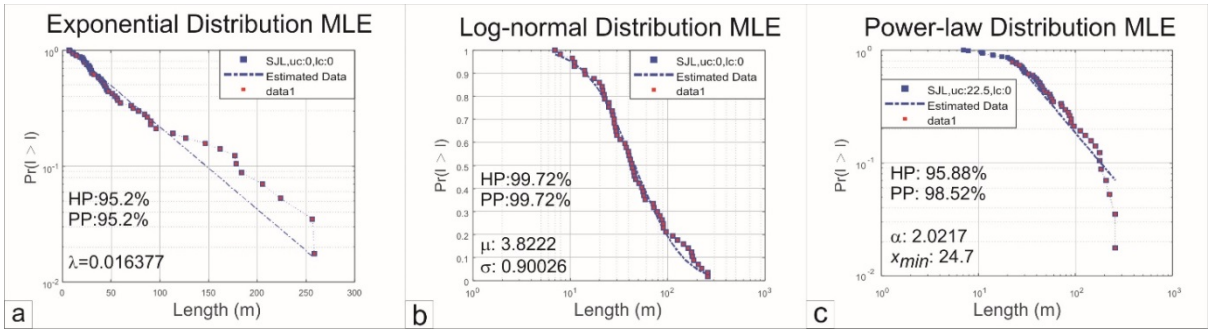

Fig. S3: MLE plot of the highest value of HP and PP for (a) exponential distribution, (b) log-normal distribution and (c) power-law distributions obtained with the minimum truncation (lc = 0; uc = 0 for exponential and log-normal and lc = 0; uc = 22.5) in the population. Dashed blue line is the fitting curve and red squares are the truncated data used for the fitting. Data are from the transect at St. John's Point (SJ) in this study.

Tab. 1: H-percentage, P-percentage and coefficients obtained by using the MLE in both un-truncated and truncated power-law population for length. EX = exponential, LN = log-normal, PL = power-law.

Length											
			BTr1	BTr2	CTr1	CTr2	TTr1	TTr2	SK	DO	SJ
Entire population	**EX**	PP	82	12.5	97.9	98.3	99.7	92.4	97.2	91.7	95.2
		HP	82	12.5	97.9	98.3	99.7	92.4	97.2	91.7	95.2
		λ:	1.3	1.1	0.4	0.6	2.4	3.2	73474.28	0.0165	0.0163
	LN	PP	95.8	98.9	97.7	99.7	99.6	96.7	99.7	98.6	99.7
		HP	95.8	89.9	97.7	99.7	99.6	96.7	99.7	98.6	99.7
		μ:	-0.9	-1.1	0.2	0.1	-1.3	-1.5	-11.42	3.7	3.8
		σ:	1.225	1.303	1.27	0.929	1.038	1.036	0.851	0.901	0.900
	PL	PP:	0	0	49.8	2.6	50.2	16.5	58.2	0.12	13.3
		HP:	0	0	64	12.6	77.5	30.6	74.6	0.56	33.8
		α:	1.3	1.2	1.4	1.49	1.5	1.4	1.5	1.4	1.5
		x_{min}	0.01	0.005	0.155	0.115	0.05	0.023	$1.5e^{-06}$	3.5	7.9

Truncated Population	**PL**	uc:	-	0	0	0	2.5	-	0	0	0
		lc:	-	30	30	30	45	-	10	15	12
		PP:		95.5	61	89.4	87.7		92.5	84.2	91.6
		HP:		97.8	77.1	94.4	94.8		97.6	95.2	97.6
		α:		1.840	1.781	2.156	2.152		1.793	1.994	1.923
		x_{min}		0.185	0.88	0.80	0.27		$3.8e^{-06}$	20.5	19.9

Tab. 2: H-percentage, P-percentage and coefficients obtained by using the MLE in both un-trucated and power-law truncated population for aperture. EX = exponential, LN = log-normal, PL = power-law.

Aperture									
			BTr1	BTr2	CTr1	CTr2	TTr1	TTr2	SK
Entire population	**EX**	PP:	54.8%	72.6%	81.9%	16.4%	99.8%	81.2%	97.8%
		HP:	54.8%	72.6%	81.9%	16.4%	99.8%	81.2%	97.8%
		λ:	197.461	482.655	341.705	263.194	1055.5947	328.879	73474.286
	LN	PP:	99.6%	99.6%	99.9%	99.3%	99.4%	99.6%	99.8%
		HP:	99.6%	99.6%	99.9%	99.3%	99.4%	99.6%	99.8%
		μ:	-6.803	-7.608	-7.289	-7.395	-7.743	-6.840	-11.42
		σ:	2	1.773	2.043	1.980	1.507	1.3055	0.851
	PL	PP:	51.7%	69.9%	82.5%	78.5%	71.1%	95.8%	52.9%
		HP:	71.2%	86.6%	82.5%	78.5%	88.1%	98.9%	74.6%
		α:	1.202	1.240	1.252	1.231	1.248	1.516	1.489
		x_{min}	$1e^{-05}$	$1e^{-05}$	$2e^{-05}$	$1e^{-05}$	$1e^{-05}$	0.0002	$1.5555e^{06}$
Truncated Population	**PL**	uc:	0	0	0	0	0	0	0
		lc:	15	15	22.5	20	27.5	0	15
		PP:	93.2%	97.4%	97.3%	95.2	97.6%	95.8%	96.4%
		HP:	98.1%	97.4%	97.3%	98.8	97.6%	98.9%	96.4%
		α:	1.414	1.454	1.4343	1.3964	1.8177	1.516	1.8781
		x_{min}	0.0002	0.0001	0.0002	0.0001	0.0003	0.0002	$4.66e^{-06}$

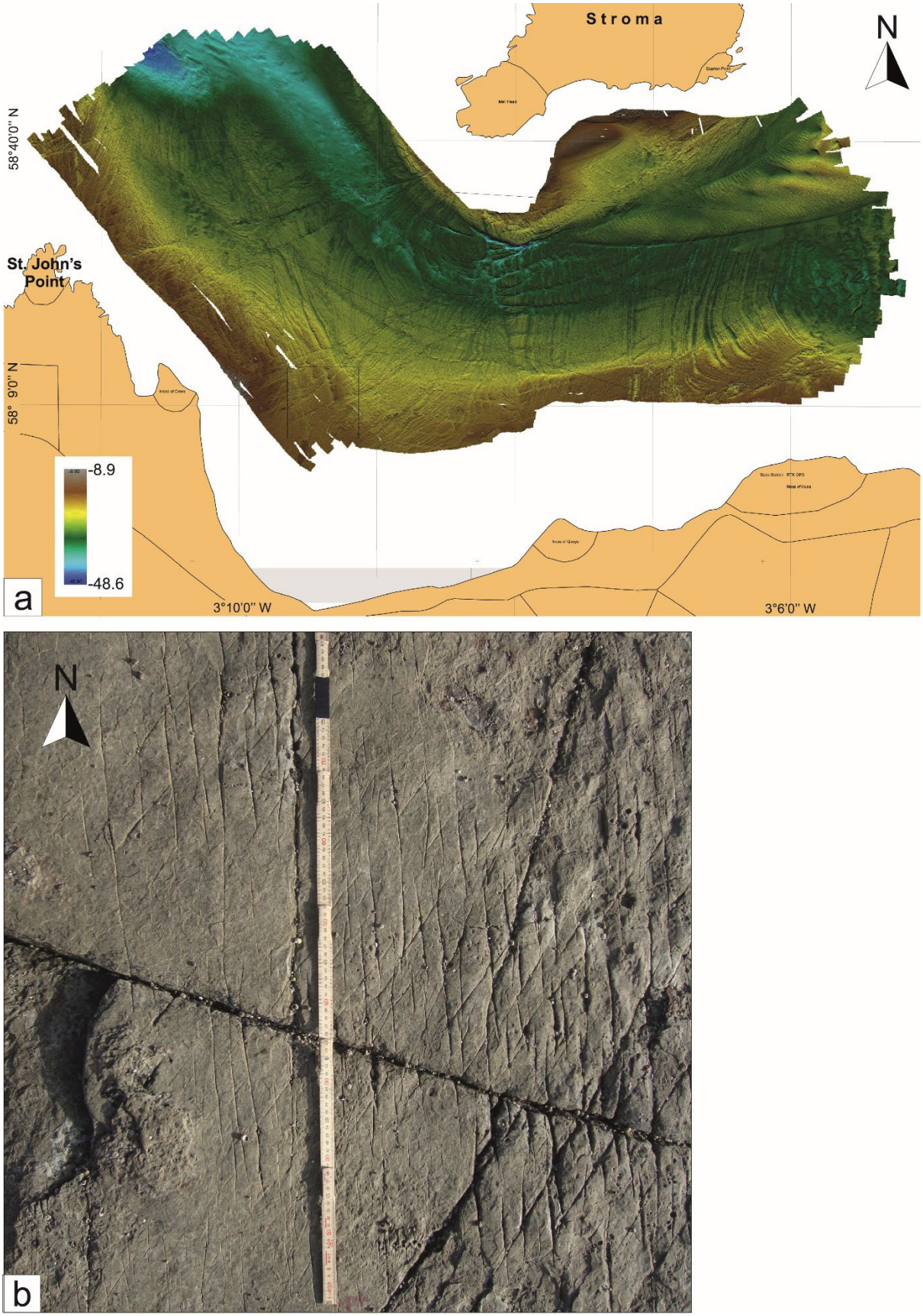

Fig. S3: Raw images used for 2D analysis: (a) Bathymetric data from the area between St. John's Point and Stroma Island and (b) outcrop pavement photograph.

Clauset, A., Shalizi, C. R. and Newman, M. E.: Power-law distributions in empirical data. SIAM review, v. 51, no. 4, p. 661-703, 2009.

Hung, H.M.J., O'Neill, R.T., Bauer, P., Kohne, K.: The behavior of the p-value when the alternative hypothesis is true. Biometrics. 53 (1): 11–22, 1997.

Healy, D., Rizzo, R. E., Cornwell, D. G., Farrell, N. J., Watkins, H., Timms, N. E., Gomez-Rivas, E. and Smith, M.: FracPaQ: A MATLAB™ toolbox for the quantification of fracture patterns. Journal of Structural Geology, v. 95, p. 1-16, 2017.

Mitzenmacher, M.: A brief history of generative models for power law and lognormal distributions. Internet mathematics, 1(2), 226-251, 2004.

Rizzo R. E., Healy, D. and De Siena, L.: Benefits of maximum likelihood estimators for fracture attribute analysis: Implications for permeability and up-scaling. Journal of Structural Geology, v. 95, p. 17-31, 2017.

APPENDIX F

Detailed Core log13z - Clair

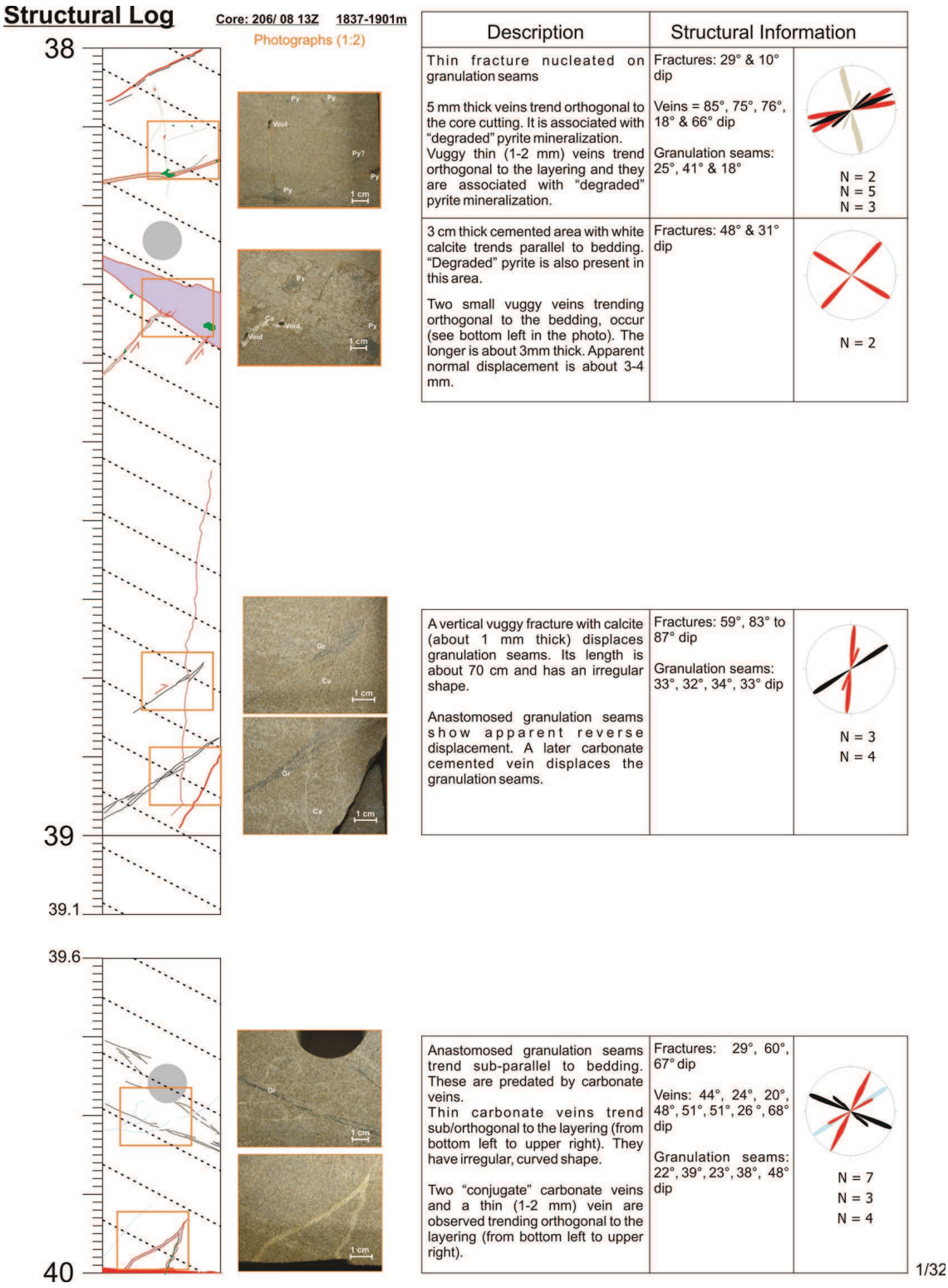

Structural Log

Core: 206/ 08 13Z 1837-1901m

Photographs (1:2)

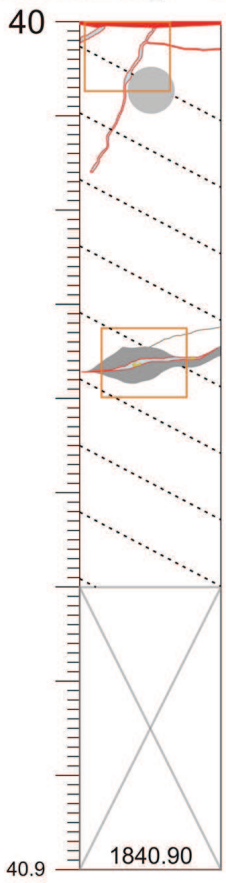

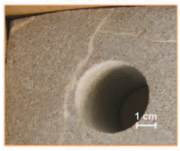

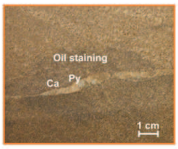

Description	Structural Information	
Two curved carbonate veins (see previous core cutting) trend sub-orthogonal to the layering.	Fractures: 30°, 62° & 5° dip	N = 3
Sigmoidal calcite vein with golden rounded pyrite "clasts" in the central part and at the edges. The thickness of calcite vein is about 5 mm in the centre. Black oil staining is observed around this vein. It has an elliptic shape.	Fractures: 32°, 20° & 0° dip Oil trail: 14° dip	N = 3 N = 1

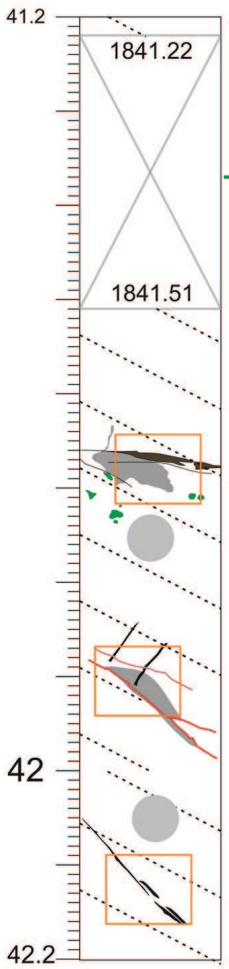

→ *Thin-section 1841.37 (2/6/2)*
"Indipendent Petrographic Services"

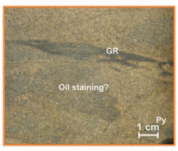

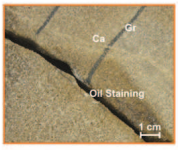

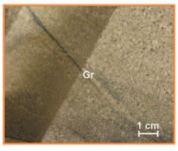

Calcite vein (1mm thick) associated with bitumen. Granulation seams trend horizontally to the core cutting. They show ribbon shape and they are associated with pyrite and oil staining (?). Rounded "clasts" of weathered pyrite also occur.	Granulation seams: 0°, 17°, 7°, 37°, 75° dip	N = 5
Two fractures trend parallel to bedding; one of them is open, the other is sealed by carbonate cement. Granulation seams have trend orthogonal to the layering from the open fracture in direction upper right. Oil staining is mainly observed at the top of the open fracture.	Fractures: 20°, 39°, 17°, 29° dip Granulation seams: 50° & 54° dip	N = 2 N = 4
Granulation seams running upper left to bottom right.	Granulation seams: 50°, 44° & 40° dip	N = 3

Structural Log

Core: 206/ 08 13Z 1837-1901m

Photographs (1:2)

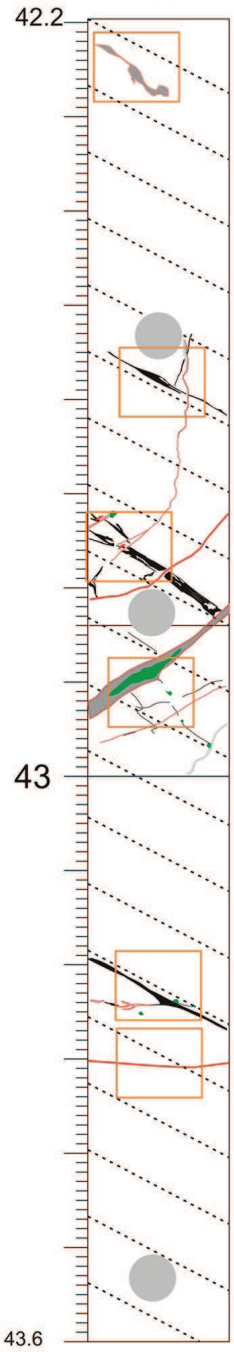

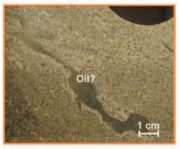

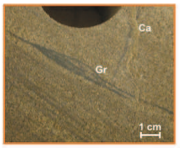

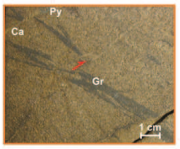

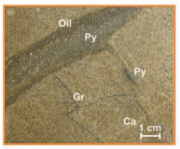

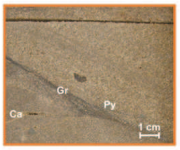

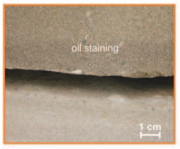

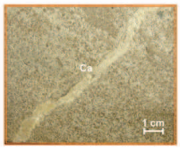

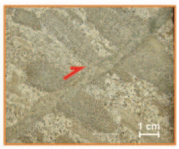

Description	Structural Information	
1-2mm thick vein runs parallel to the cutting and shows an irregular shape. This vein displaces granulation seams in 3 points (5 mm apparent reverse offset). Granulation seams trend parallel to the layering and they show a anastomosed shape. Gouge with oil staining and pyrite occur orthogonal to the layering. Thin granulation seams with irregular shape trend from top left to bottom right. Small clasts (<1mm) of degraded pyrite are associated with one of them.	Granulation seams: 27°, 31°, 39°, 21°, 19°, 4°, 7°, 6° dip Fractures: 84°, 87°, 50°, 36°, 24°, 30°, 50°, 35°, 20°, 7°, 27°, 40°, 70°, 27°, 33°, 30°	N = 16 N = 8
Granulation seam trends parallel to layering. It is partially reactivated and associated with calcite and small clasts of degraded pyrite. A fracture orthogonal to the core represent a barrier to oil.	Fractures: 1°, 5°, 6° dip Granulation seams: 1°, 30° dip	N = 3 N = 2
1 cm thick carbonate vein with irregular shape trends orthogonally to the layering.	Fractures: 44	N = 1
1 cm thick carbonate vein with irregular shape trend orthogonally to the layering and it shows 1 cm of apparent reverse displacement	Fractures: 77°, 37° dip	N = 2

Structural Log

Core: 206/ 08 13Z 1837-1901m

Photographs (1:2)

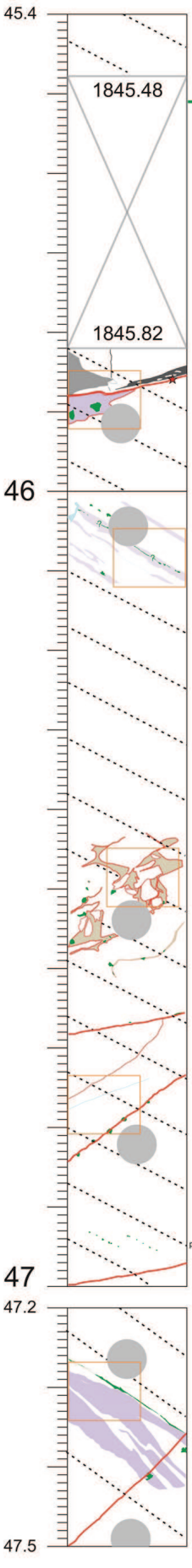

Thin-section 1845.51 (2/7/1)
"Indipendent Petrographic Services"

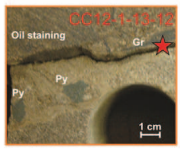

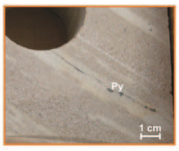

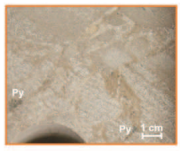

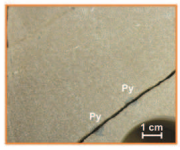

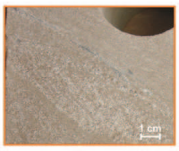

Description	Structural Information	
Subhorizontal fracture reactivated a granulation seams observed at the top right Oil staining is observed in the upper left. A small region made of cemented sandstones with rounded clasts of degraded pyrite occurs under the fracture.	Fractures: 11°, 7°, 13° dip Granulation seams: 88°, 16°, 9°, 89° dip	N = 3 N = 4
Alternated regions of darker and lighter bands occur (different cement ?). In the lighter regions a thin fracture with degraded pyrite occur.		
Complex brecciated region underlined by the different cement. Small pyrite have been observed associated mainly with the cemented areas.	Fractures: 12°, 24°, 16°, 36°, 27°, 22° dip	N = 6
Four fractures trrend top right to bottom left and show the presence of pyrite (golden on the fresh surface). 1mm thin carbonate vein trends bottom left to upper right	Fractures: 9°, 9°, 38° dip	N = 3
Region with sedimentary carbonate cement. At the top of this region has been observed a thin elongate region with green degraded pyrite. Fracture trends bottom left to top right	Fractures: 42°, 45°, 64° dip	N = 3

Structural Log

Core: 206/ 08 13Z 1837-1901m

Photographs (1:2)

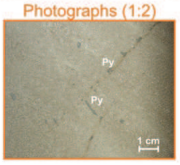

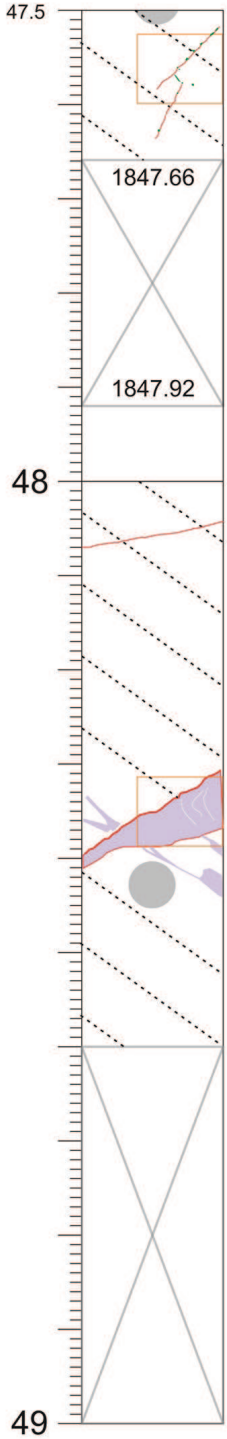

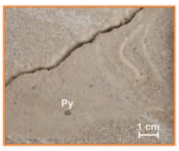

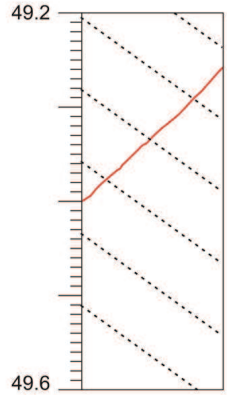

Description	Structural Information	
Two thin fractures are associated with carbonate cement and "degraded" pyrite		
Fracture orthogonal to the core cutting.	Fractures: 7° dip	N = 1
Fracture associated with finer sandstone which show some soft sediment deformations. The contact at the bottom of this area creates an angle of 30° with the layering, while the contact at the top is marked by a fracture at 60° to bedding.	Fractures: 31, 16, 34° dip	N = 3
Fracture trending orthogonal to the layering	Fractures: 42° dip	N = 1

Structural Log

Core: 206/ 08 13Z 1837-1901m

Photographs (1:2)

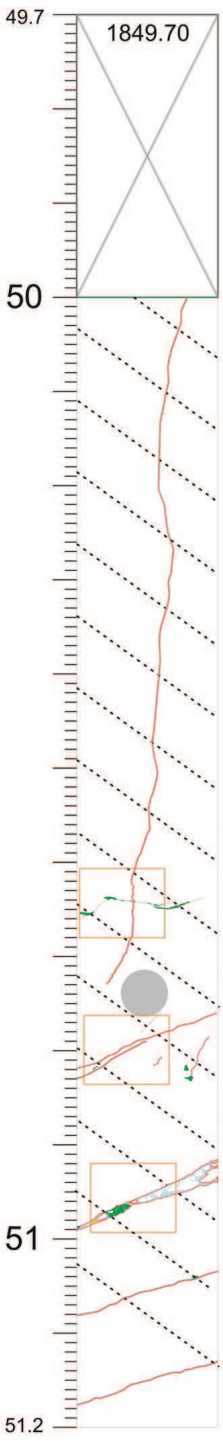

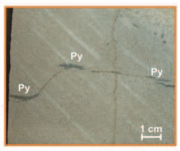

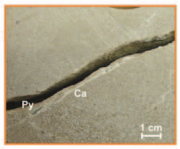

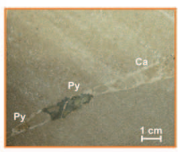

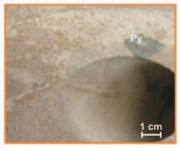

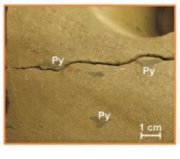

Description	Structural Information	
	Fractures: 65, 84, 60, 86, 87° dip	N = 5
A vertical and partially cemented fracture is more than 1m long. Thin fracture orthogonal to the core cutting with “S shape” shows pyrite mineralization at the fracture bends. Four parallel carbonate veins occur. They are 1 to 3 mm thick. One of them is open and associated with carbonate infil. Pyrite occurs associated with a calcite filled fractures.	Fractures: 45, 20, 29, 67, 23, 15, 15, 16° dip	N = 8
Large cemented regions with pyrite	Fractures: 10°, 14°, 25°, 5°, 5°, 15°, 75°, 90°, 23° dip	N = 8
Fracture trending subhorizontal to the core cutting. Small pyrite (<5mm) is observed along the fracture and parallel to bedding	Fractures: 7° dip	N = 1

Structural Log

Core: 206/ 08 13Z 1837-1901m

Photographs (1:2)

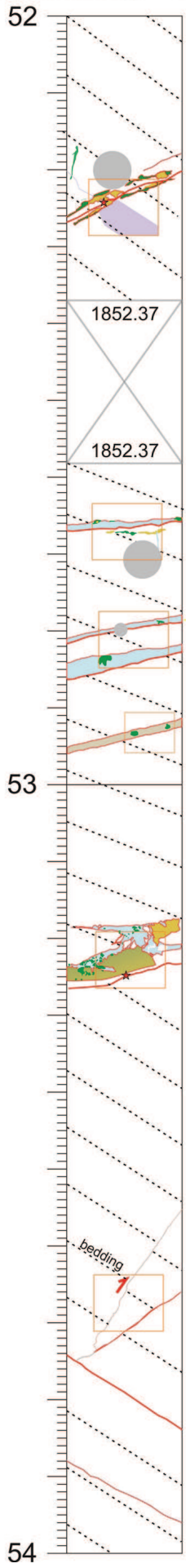

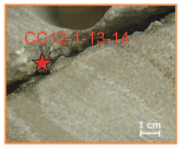

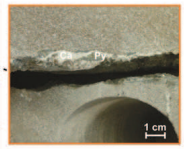

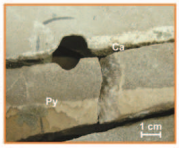

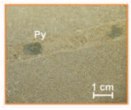

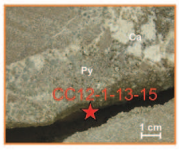

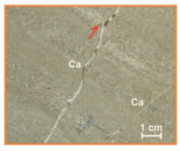

Description	Structural Information	
Fracture oriented at 45° to the bedding with fresh golden pyrite and calcite (sampled).	Fractures: 29°, 20°, 9°, 31° dip	N = 4
Fracture with 5mm thick carbonate mineralization and golden pyrite sub-horizontal to the core cutting A 2mm thin vein trends vertically to join the fracture. Parallel to these fractures, a region with altered calcite cement occurs. It is fractured at its bottom edge where golden pyrite occurs. 6mm of darker sandstones (different cement ?) has the same trend of previous fractures. Two degraded and rounded clasts of pyrite are also present there.	Fractures: 5°, 5°, 17°, 15°, 15°, 15° dip	N = 6
Breccia with golden, fresh pyrite, degraded pyrite and carbonate cement	Fractures: 4°, 8°, 18°, 5°, 10° dip	N = 5
Two fractures orthogonal to the core cutting occur. They are carbonate filled terminates on a parallel bedding fracture. One of these fractures shows apparent reverse offset. Two fractures sub-parallel to bedding occur.	Fractures: 54°, 35°, 34°, 28° dip	N = 4

Structural Log

Core: 206/ 08 13Z 1837-1901m

Photographs (1:2)

54

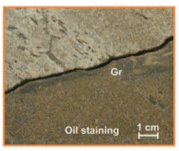

Curved fracture oriented at low angle to the layering

Fracture parallel to bedding

Fracture at a low angle to the bedding. It represents a good conduit for fluid along the fracture and a barrier across the fracture. Oil occur along the fracture and at the bottom.

Fractures: 6°, 19°, 32°, 18° dip

N = 4

55

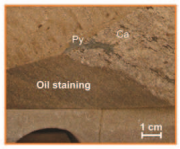

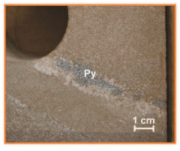

Cemented stratigraphic layers (lighter) associated with degraded elongate clasts of pyrite.

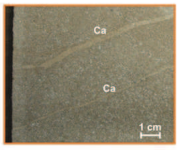

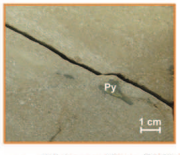

Fractures with carbonate mineralization occur. Thickness is about 0.5 mm.
Small clasts of degraded pyrite are not associated with fractures or veining.

Fracture parallel bedding occurs. Elongate clasts of pyrite have been observed below it.

Fractures: 5°, 17°, 17°, 37° dip

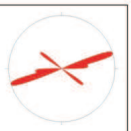

N = 4

Thin-section 1856.96 (3/4/2)
"Indipendent Petrographic Services"

56

Structural Log

Core: 206/ 08 13Z 1837-1901m

Photographs (1:2)

Description	Structural Information
The fracture in direction bottom left to upper right are partially associated with carbonate mineralization (2mm thin). Another fracture is parallel to the bedding and terminated on the previous one. Degraded pyrite is observed at the intersection between the two fractures.	Fractures: 19°, 38°, 24°, 15°, 19°, 15°, 7°, 5°, 7° dip

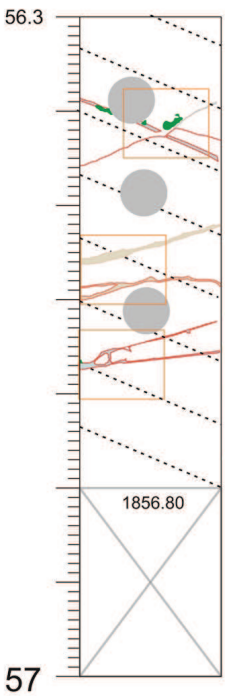

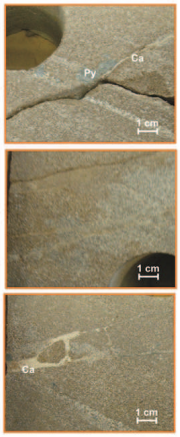

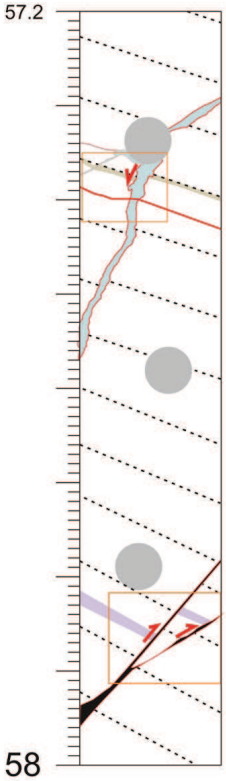

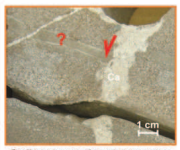

Sedimentary carbonate cement -> Carbonate veins

Carbonate filled fractures normally displace the layers	Fractures: 29, 32, 17, 20, 42, 75, 63° dip	N = 6

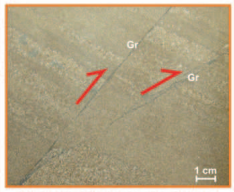

Sedimentary carbonate cement -> Bitumen

Granulation seams orthogonal to the bedding and showing reverse displacement.	Fractures: 49, 31, 38, 24° dip	N = 4

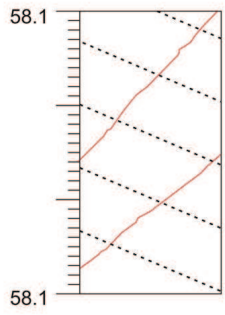

2 fractures sub-orthogonal to the layering.	Fractures: 45°, 38° dip	N = 2

Structural Log

Core: 206/ 08 13Z 1837-1901m

Photographs (1:2)

Description	Structural Information
	Fractures: 45°, 38° dip

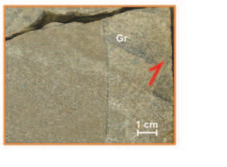

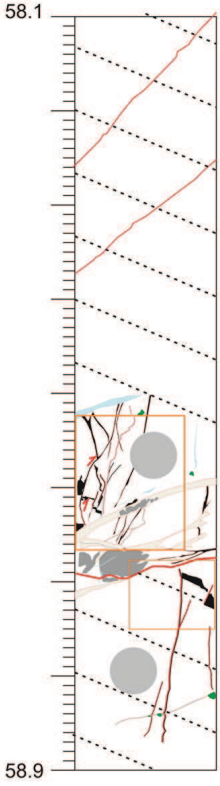

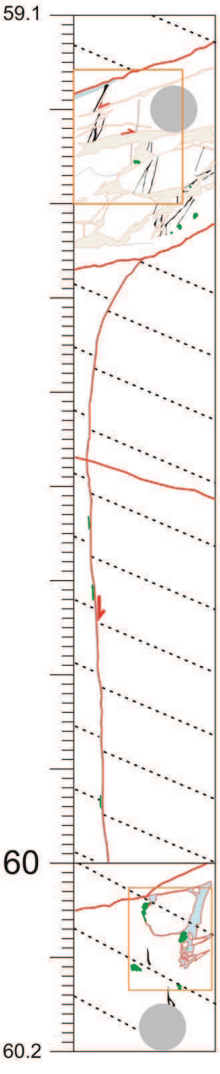

	Fractures: 76, 53, 77, 61, 73, 77, 80, 75, 81, 65, 74, 68, 76, 70, 68, 58, 22, 22, 17, 32, 81, 12, 12, 16, 24, 28, 86, 66, 82, 24, 74, 85° dip

oil -> calcite -> "degraded" carbonate veins

Deformed sandstones contrast due probably to calcite cement and grainsize. The oil trail is cutted by these veins.	Fractures: 26, 9, 17, 17, 25, 70, 83, 5, 11, 11, 30, 65, 45, 47, 24, 54° dip

	Fractures: 18°, 88° dip

	Fractures: 10°, 24°, 44°, 7°, 7°, 8°, 17°, 37°, 11°, 72°, 80° dip

Structural Log

Core: 206/ 08 13Z 1837-1901m

Photographs (1:2)

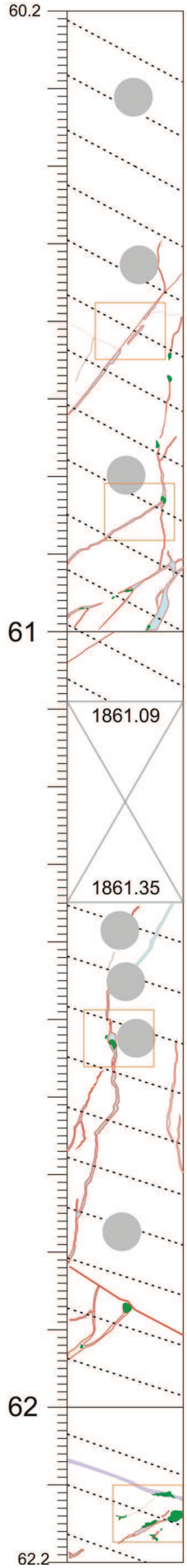

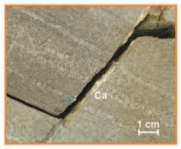

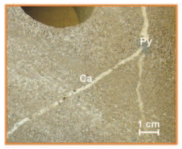

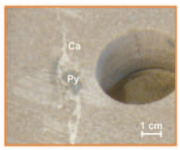

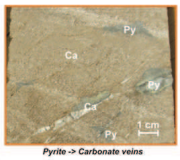

Pyrite -> Carbonate veins

Description	Structural Information	
Carbonate vein (2mm thick) oriented orthogonal to the layering and showing tensile behaviour. Thin (< 0.5 cm) carbonate veins associated with pyrite	Fractures: 50, 24, 61, 2, 76, 81, 81, 90, 29, 45, 83, 29, 45, 83, 29, 50, 64, 48, 54, 34° dip	N = 17
4mm thick vein with apparent reverse displacement (?) It is associated with weatered pyrite areas.	Fractures: 66, 61, 85, 64, 82, 81, 88, 52, 75, 85, 33, 38, 15° dip	N = 13
	Fractures: 27°, 40°, 31°, 30°, 30°, 44° dip	N = 6

Structural Log

Core: 206/ 08 13Z 1837-1901m

Photographs (1:2)

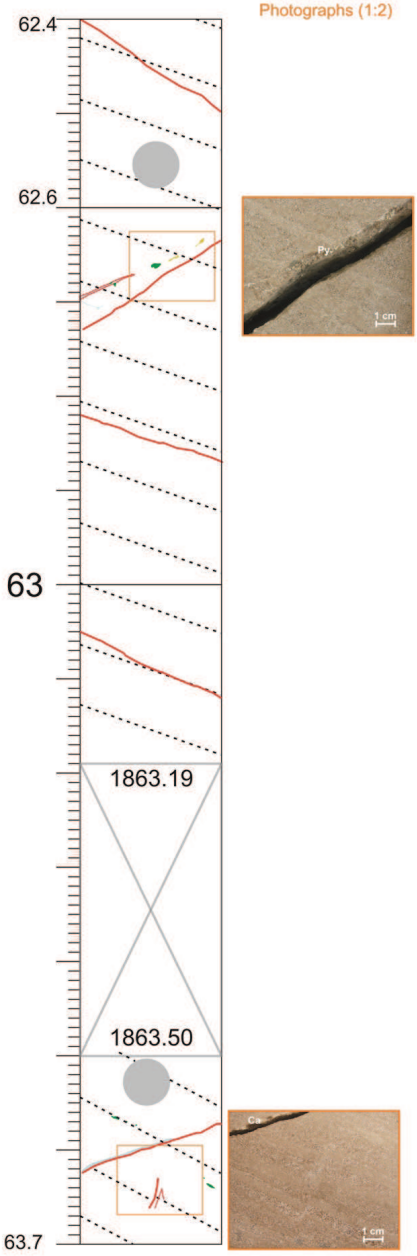

Description	Structural Information
	Fractures: 32° dip N = 1
	Fractures: 23°, 33° dip N = 2
	Fractures: 14° dip N = 1
	Fractures: 22° dip N = 1
	Fractures: 17°, 61°, 82° dip N = 3
	Fractures: 10° dip N = 1
	Fractures: 12° dip N = 1

Structural Log

Core: 206/ 08 13Z 1837-1901m

Photographs (1:2)

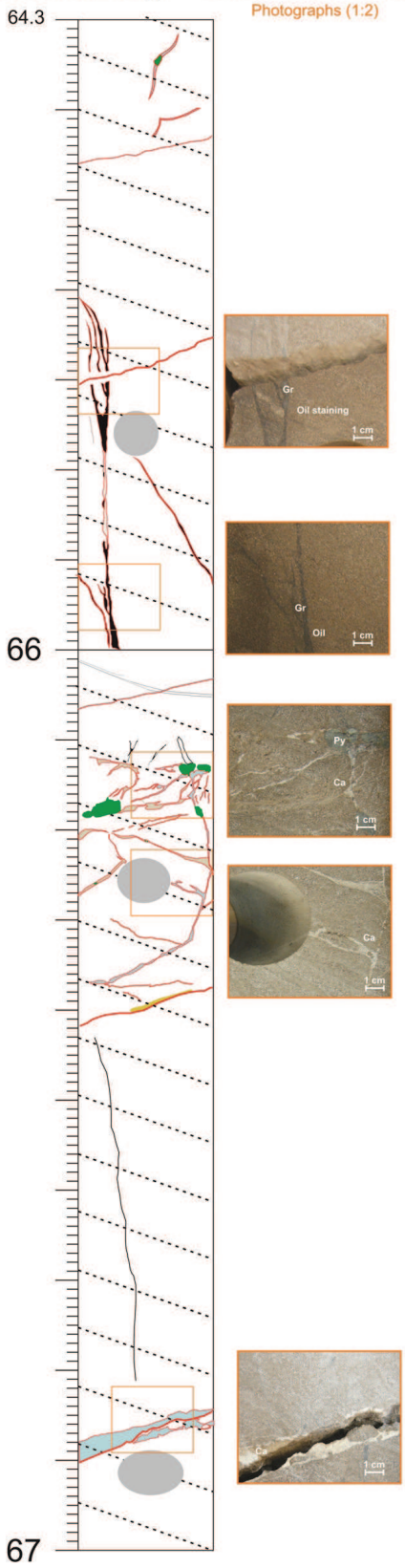

Description	Structural Information	
	Fractures: 10°, 67°, 26°, 5°, 83°, 33°, 64° dip	N = 7
Fracture cutting granulation seams and showing oil staining at its bottom (footwall)	Fractures: 17, 62, 78, 9, 9, 76, 57, 79	N = 8
Calcite along fracture (similar trend of 51-52) with some sand clasts (breccia). Thin vein (top) (with 3-4mmclasts of pyrite) has the same trend of previous to subvertical.	Fractures: 11, 11, 10, 7, 16, 40, 80, 80, 78, 13, 17, 25, 57, 47, 29, 75, 30, 13, 24, 12, 17, 17° dip Oil trails: 20, 8, 51, 65, 85, 88, 90,	N = 7 N = 21
Large fracture with breccia and with thick (>1cm) carbonate mineralization	Fractures: 20°, 30°, 10°, 14°, 12° dip	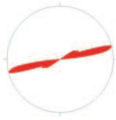 N = 5

Structural Log

Core: 206/ 08 13Z 1837-1901m
Photographs (1:2)

Description	Structural Information
Granulation seams parallel to the layering (top) and also orthogonal to the core cutting. A fracture with carbonate infil displaces the latter. Pyrite is associated with carbonate mineralization.	Fractures: 25, 25, 20, 26, 83, 81, 12, 14, 25 Oil trail: 29, 24, 72, 65, 75, 85, 59, 66, 69, 73, 80, 80, 78, 67, 68° dip

67.3

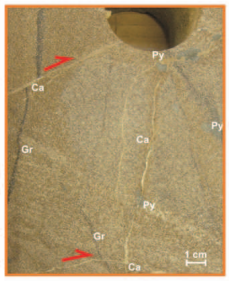

N = 9
N = 15

67.7

68

★ CC12-1-13-05

Fractures: 2° dip

N = 1

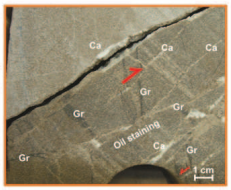

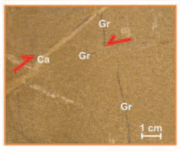

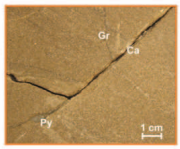

Crosscutting relationship showing granulation seams repeatedly cut by mainly tensile carbonate veins.

Fractures: 32°, 45°, 45°, 30°, 39°, 30°, 41°, 46°, 35°, 44°, 39°, 30°, 42°, 22° dip

Oil trails: 35, 58, 58, 98, 11, 80, 85, 88, 82, 81, 37, 69, 77, 77, 38, 17, 81, 71, 53, 53, 88, 72

Veins: 6, 28, 45, 41, 33, 37, 22

N = 14
N = 21
N = 7

1856.81

69

69.3

Fractures: 10°, 23° dip

N = 2

69.5

69.8

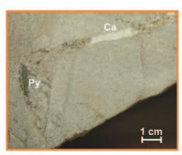

Fractures: 13°, 22°, 70°, 81°, 29°, 23°, 24° dip

N = 7

70

Structural Log

Core: 206/ 08 13Z 1837-1901m

Photographs (1:2)

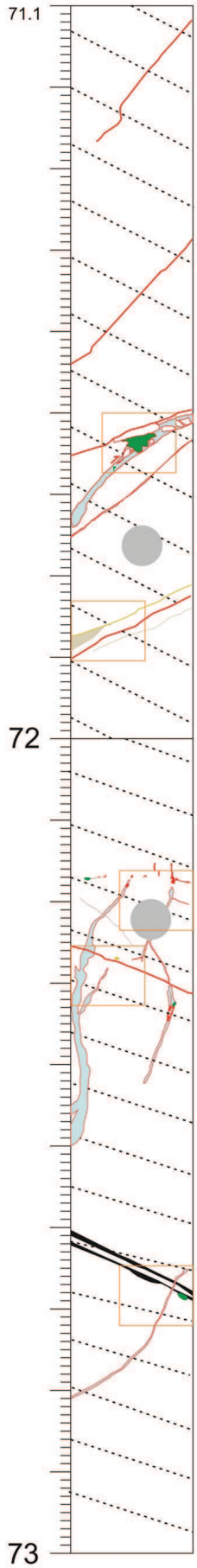

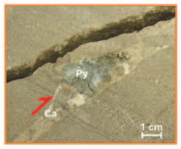

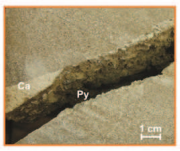

Photographs (1:2)

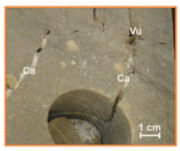

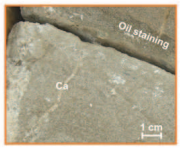

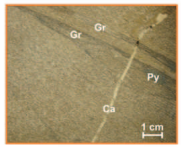

Description	Structural Information	
	Fractures: 52°, 42°, 89° dip	N = 3
	Fractures: 47°, 30° dip	N = 2
	Fractures: 30°, 19°, 17°, 33°, 18°, 15°, 37°, 41° dip	N = 8
	Fractures: 32°, 19°, 25°, 35° dip	N = 4
	Fractures: 14°, 87°, 64°, 74°, 57°, 9°, 44°, 70°, 19°, 44°, 33°, 54°, 73°, 82°, 70°, 36°, 63°, 19° dip	N = 18
Granulation seams cut by tensile vein	Fractures: 64°, 36°, 30°, 44° dip Oil trail: 26° ,22° ,27° dip	N = 3 N = 4

Structural Log

Core: 206/ 08 13Z 1837-1901m

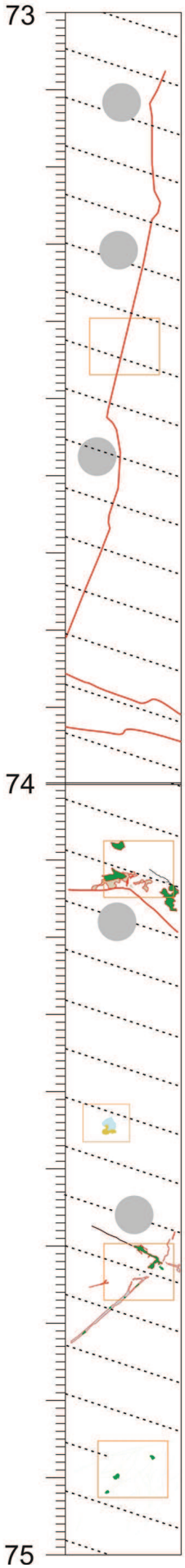

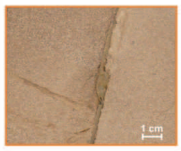

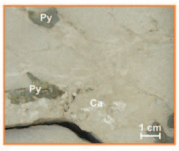

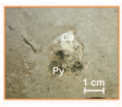

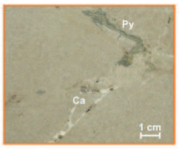

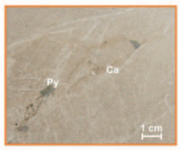

Description	Structural Information	
Fracture orthogonal to the layering which cuts the core for about 80cm	Fractures: 66°, 89°, 78°, 68°, 72°, 88°, 41° dip	N = 7
Curved fractures sub-parallel to the layering	Fractures: 21°, 34°, 17°, 7°, 21°, 53° dip	N = 6
	Fractures: 1°, 5°, 42°, 65°, 18° & 9° dip	N = 6
Carbonate mineralization occurring along a fracture orthogonal to the layering and pyrite in a fracture sub-parallel to the layering.	Fractures: 27°, 41°, 15°, 71°, 61°, 64°, 44°, 36° dip	N = 8
	Fractures: 24°, 13°, 12°, 57°, 44°, 46°, 77°, 43°, 44°, 71°, 88°, 67°, 34°, 41°, 66°, 34°, 59°, 43°, 65°, 49°, 79°, 58°, 89° dip	N = 23

Structural Log

Core: 206/ 08 13Z 1837-1901m

Photographs (1:2)

Description	Structural Information	
Fracture with pyrite (< 1cm thick) and calcite infil. Minor fracture terminate on it.	Fractures: 21°, 49°, 18°, 64°, 85°, 76°, 89° dip	N = 7
Fracture with thin carbonate mineralization	Fractures: 36° dip	N = 1
Fracture with pyrite infil (< 0.8 cm thick)	Fractures: 25° & 13° dip	N = 2
	Fractures: 20°, 31°, 21°, 13° dip	N = 4
Carbonate veins oriented parallel and orthogonal to the layering	Fractures: 54°, 35°, 36°, 69°, 72°, 25°, 28°, 25°, 25°, 19° dip	N = 10

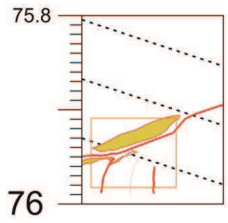

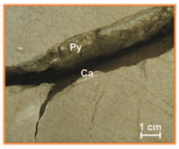

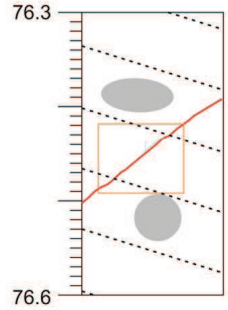

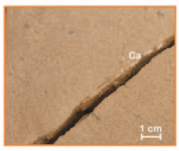

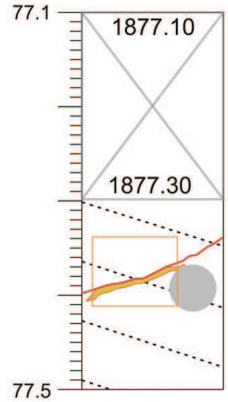

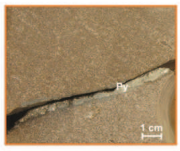

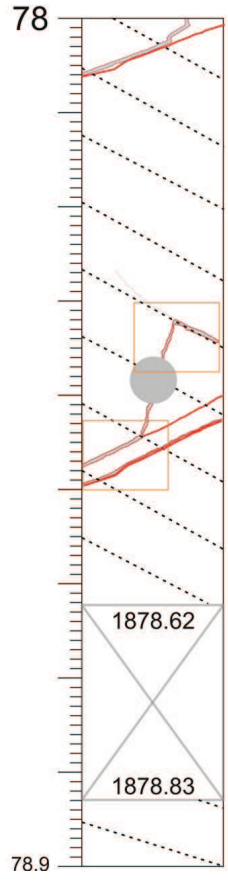

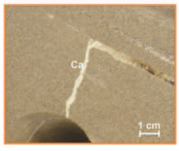

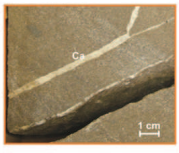

Structural Log

Core: 206/ 08 13Z 1837-1901m

Photographs (1:2)

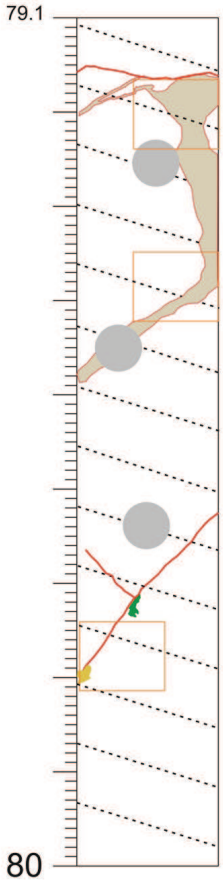

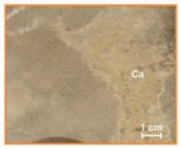

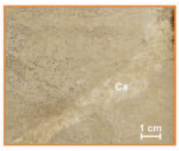

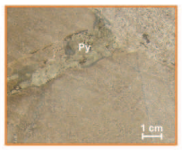

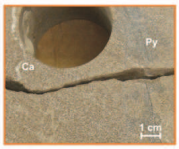

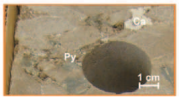

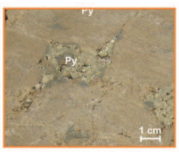

Description	Structural Information	
	Fractures: 32°, 13°, 8°, 22°, 28°, 17°, 34°, 76° dip	N = 8
Fault orthogonal to the layering associated with pyrite mineralization	Fractures: 46°, 44°, 54° dip	N = 3
Pyrite at the contact between	Fractures: 10°, 8° & 27° dip Granulation seams: 88°, 85°, 79°, 76°, 82° dip Veins: 23°, 58°, 66°, 12°, 85°, 83°, 83°, 69°, 74°,73° dip	N = 3 N = 5 N = 11
Pyrite mainly localized at the intersection between fractures orthogonal to the layering and carbonate cemented fractures parallel to the layering	Fractures 1: 19, 7, 15, 23, 17, 1, 36, 35, 38, 9, 22, 67, 45, 57, 56, 57, 30 Fractures 2: 15, 44, 20, 25, 32, 62, 37, 15, 21 Fractures 3: 29, 6, 6, 57, 34, 29, 23, 18, 10, 78, 94, 58, 58, 34, 18, 61	N = 17 N = 9 N = 16

Structural Log

Core: 206/ 08 13Z 1837-1901m

Photographs (1:2)

Description	Structural Information
Fault breccia made of clasts of host rocks, pyrite and calcite.	Fractures: 38°, 16°, 26°, 76°, 36°, 6°, 52°, 17°, 35°, 17° & 5° dip Granulation seams: 24°, 55°, 58°, 19°, 41°, 15° dip

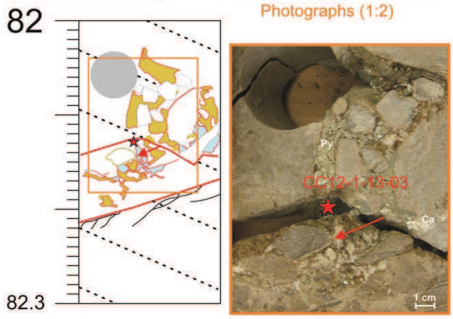

82.7

1882.73

83

Thin-section 1882.92 (4/3/1)
"Indipendent Petrographic Services"

83.4

83.5

Fractures: 28° dip

83.8

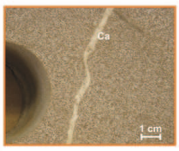

Fractures: 19°, 61°, 78°, 31°, 7°, 19° dip

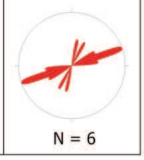

84

1884.07

Thin-section 1884.12 (4/4/2)
"Indipendent Petrographic Services"

Thin-section 1884.30 (4/4/3)
"Indipendent Petrographic Services"

1884.35

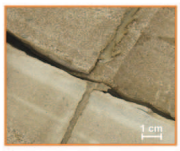

Fractures: 57°, 57°, 35° & 68° dip

Fractures: 53°, 45°, 69°, 57° dip

84.9

Structural Log

Core: 206/ 08 13Z 1837-1901m

Photographs (1:2)

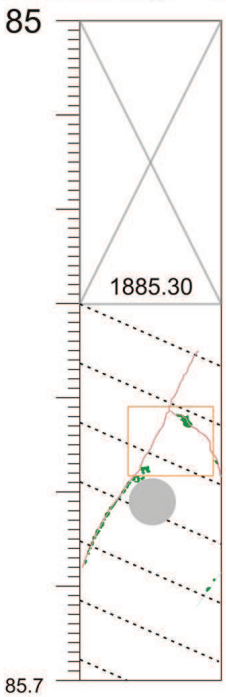

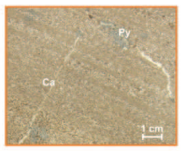

Description	Structural Information	
	Fractures: 69°, 47°, 56°, 63° dip	N = 4

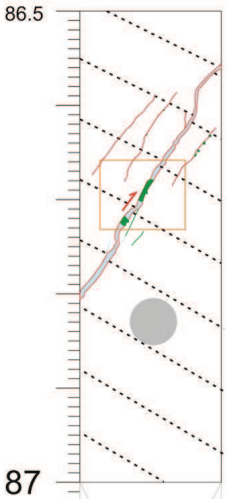

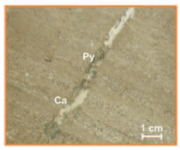

Description	Structural Information	
Carbonate-infilled fractures (+ pyrite) orthogonal to the layering and with apparent reverse displacement.	Fractures: 87°, 86°, 51°, 51°, 49°, 85°, 55°, 52°, 52° dip	N = 8

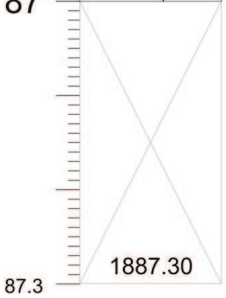

CC12-1-13-06

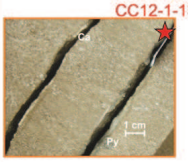

Description	Structural Information	
Carbonate-infilled fractures (+ pyrite) orthogonal to the layering.	Fractures: 53°, 53°, 70° dip	N = 3

Structural Log

Core: 206/ 08 13Z 1837-1901m

Photographs (1:2)

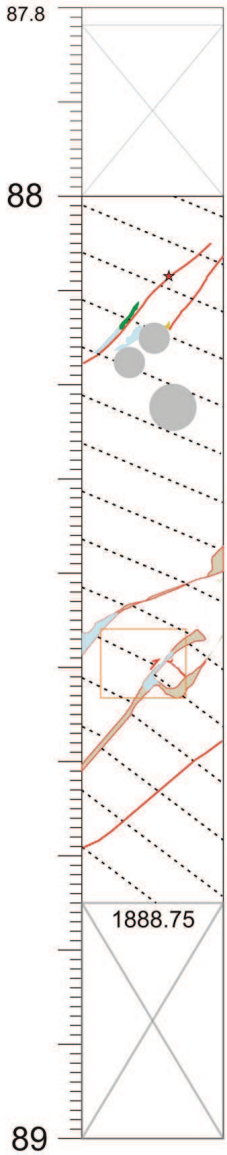

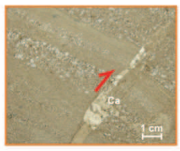

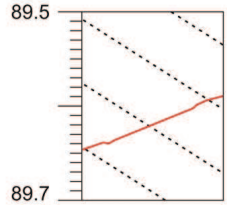

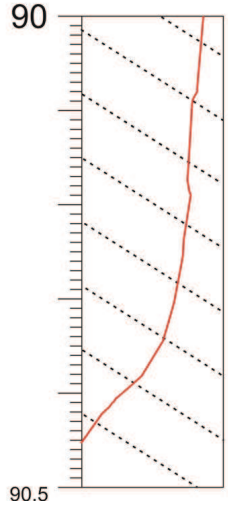

Description	Structural Information	
Carbonate-infilled fractures (+ gold pyrite) orthogonal to the layering.	Fractures: 42°, 53° & 40° dip	N = 3
Carbonate-infilled fractures orthogonal to the layering and with apparent reverse displacement.	Fractures: 39°, 53°, 42°, 40°, 50°, 51°, 21° dip	N = 7
	Fractures:° dip	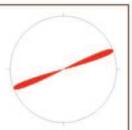 N = 1
	Fractures: 87°, 83°, 57°, 42°, 58° dip	N = 5

Structural Log

Core: 206/ 08 13Z 1837-1901m

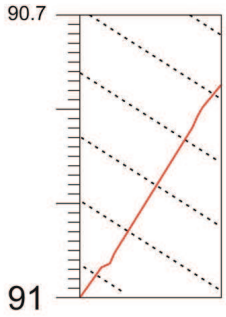

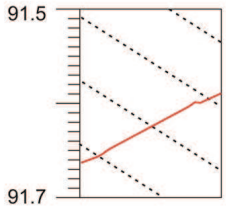

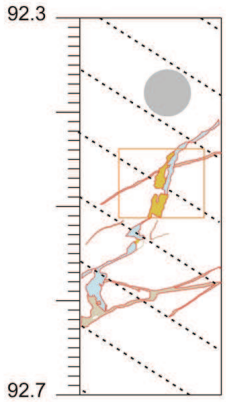

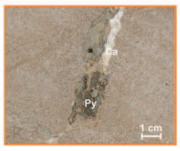

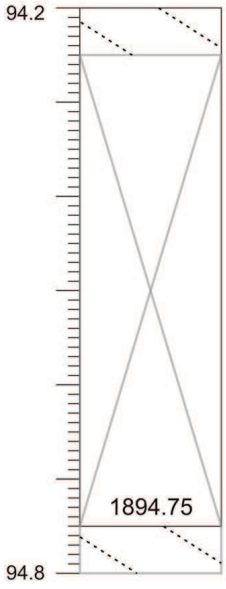

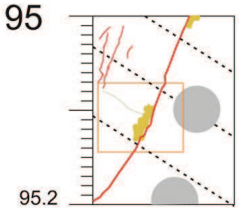

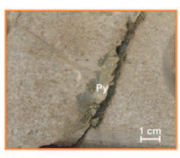

Description	Structural Information	
	Fractures: 58° dip	N = 1
	Fractures: 27° dip	N = 1
Carbonate-infilled fractures (+ pyrite) orthogonal to the layering.	Fractures: 31°, 31°, 74°, 18°, 47°, 66°, 19°, 42°, 72°, 21°, 13°, 8°, 33°, 25°, 25° dip	N = 15
Fractures with gold pyrite mineralization orthogonal to the layering.	Fractures: 68°, 68°, 82° & 51° dip Veins: 36° & 52° dip	N = 2 N = 4

Structural Log

Core: 206/ 08 13Z 1837-1901m

Photographs (1:2)

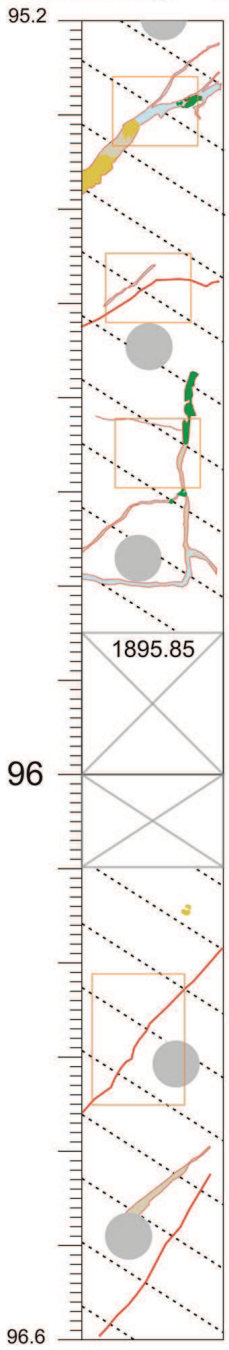

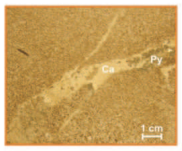

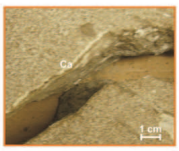

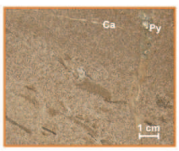

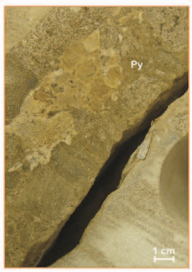

Description	Structural Information	
Carbonate-infilled fractures (+ pyrite) orthogonal to the layering.	Fractures: 50°, 36°, 56°, 38°, 14°, 46°, 66°, 23° dip	N = 8
	Fractures: 35°, 38°, 2°, 22°, 31° & 6° dip	N = 6
	Fractures: 21°, 85°, 67°, 100°, 87°, 52°, 42°, 1° & 3° dip	N = 9
	Fractures: 44°, 57°, 57°, 48°, 38°, 45° dip	N = 6
	Fractures: 22°, 35°, 19°, 10°, 41° & 72° dip	N = 6

Structural Log

Core: 206/ 08 13Z 1837-1901m

Photographs (1:2)

98

99

1900

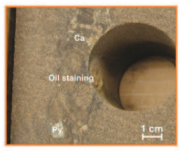

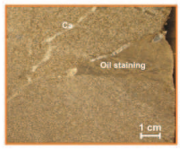

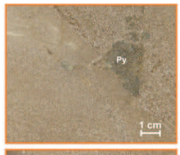

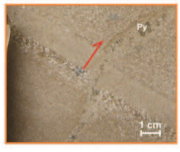

Description	Structural Information
	Fractures: 45°to 56° dip N = 2
	Granulation seams: 34° dip N = 1
	Fractures: 77°, 26°, 0°, 19°, 10°, 38, 32°, 21°, 9°, 32° dip Veins: 22° dip N = 10 N = 1
	Fractures: 24° dip N = 1
	Fractures: 20°, 24°, 42°, 29°, 71°, 5°, 5°, 13° dip N = 8
	Fractures: 30°, 47°, 30°, 36°, 73°, 62°, 80°, 20° dip N = 8

Structural Log

Core: 206/ 08 13Z 1837-1901m

Photographs (1:2)

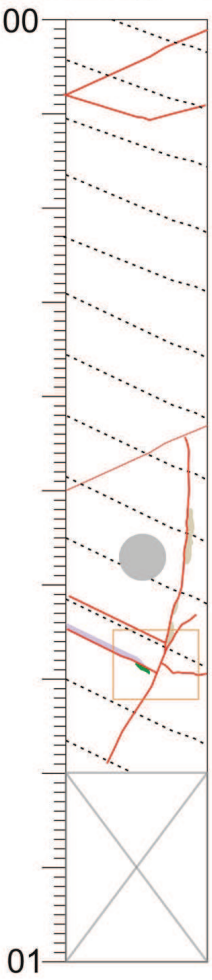

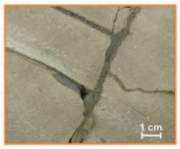

Description	Structural Information
	Fractures: 23°, 27° & 14° dip N = 3
	Fractures: 24°, 88°, 73°, 57°, 64°, 26°, 60°, 37° dip N = 8

Legend

- Gap
- Fault / Fracture
- Bedding
- Granulation seams
- Carbonate Vein
- "Degraded" Carbonate Veins
- Void
- Sedimentary Carbonate Calcite
- Oil Staining
- Pyrite
- "Degraded" Pyrite
- Sample core
- Sample for geochemical dating

Fractures

N = 592

Granulation seams

N = 94

Veins

N = 56

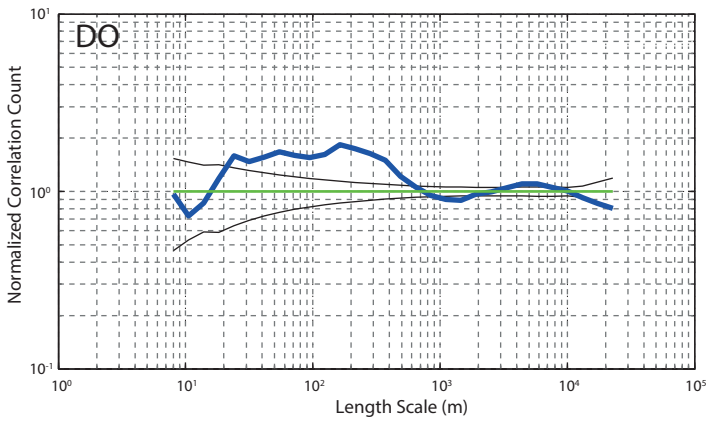
DO
Normalized Correlation Count
Length Scale (m)

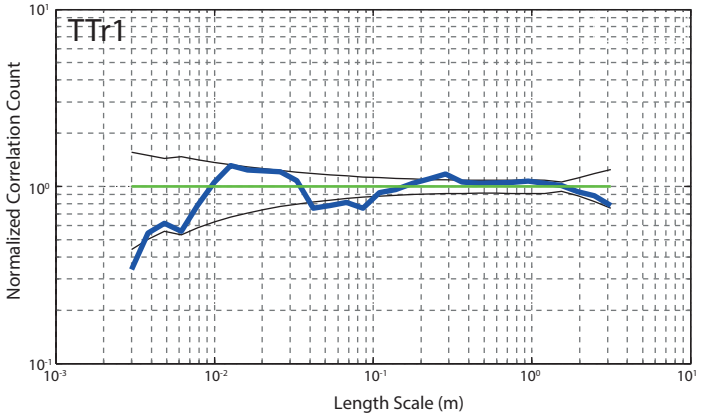
TTr1
Normalized Correlation Count
Length Scale (m)

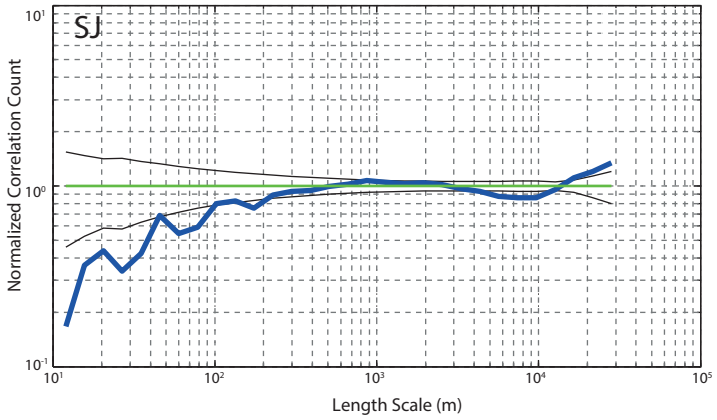
SJ
Normalized Correlation Count
Length Scale (m)

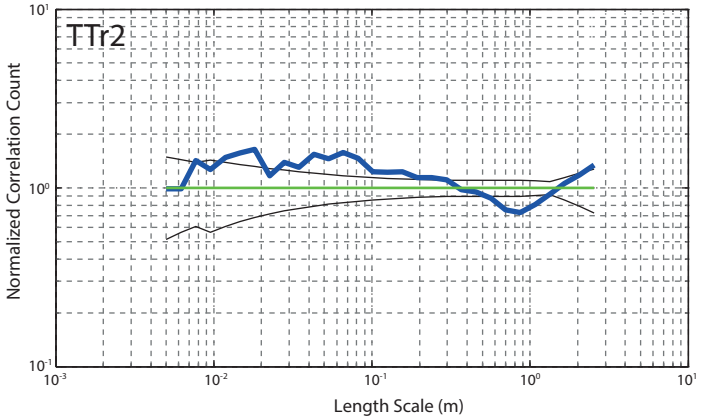
TTr2
Normalized Correlation Count
Length Scale (m)

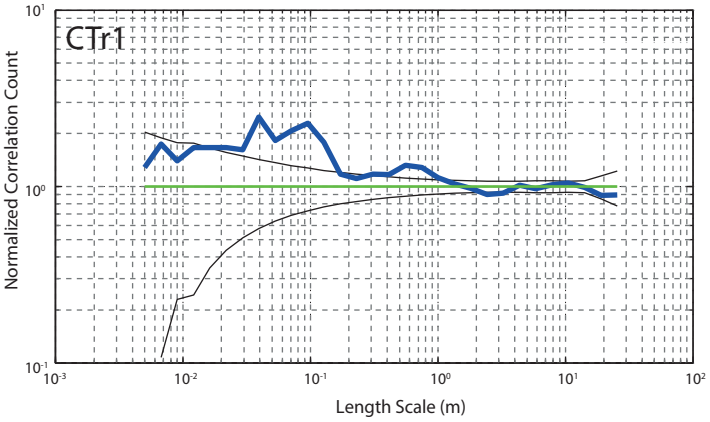
CTr1
Normalized Correlation Count
Length Scale (m)

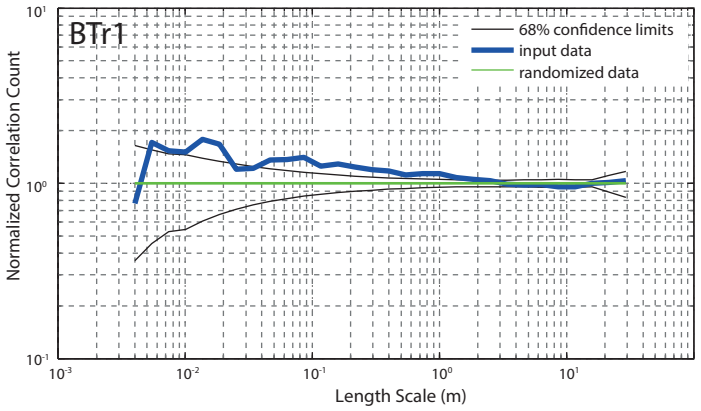
BTr1
68% confidence limits
input data
randomized data
Normalized Correlation Count
Length Scale (m)

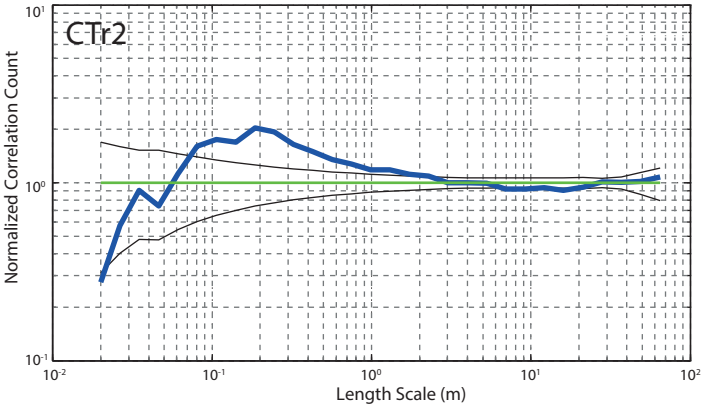
CTr2
Normalized Correlation Count
Length Scale (m)

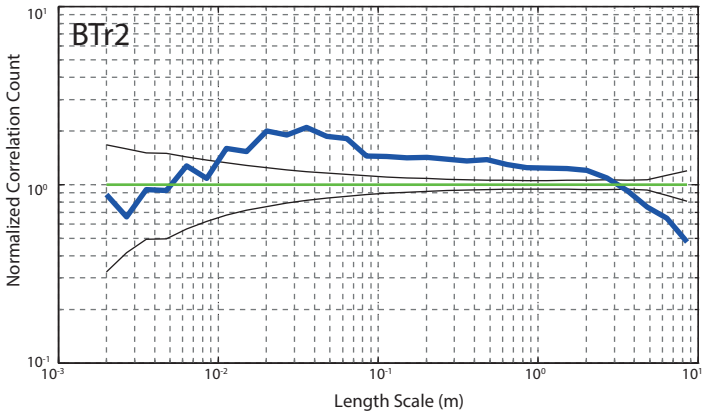
BTr2
Normalized Correlation Count
Length Scale (m)

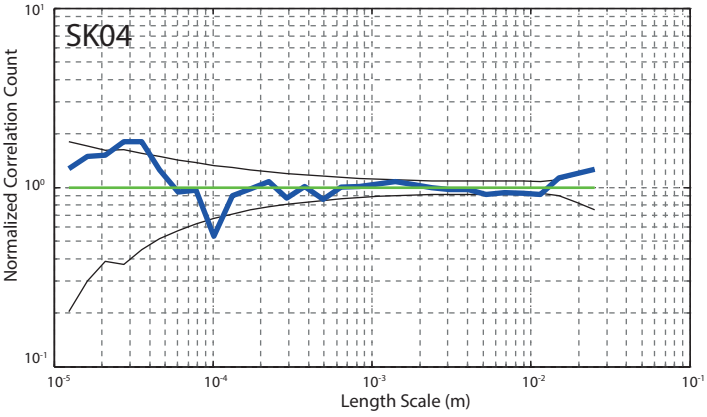
SK04
Normalized Correlation Count
Length Scale (m)